数理解析研究所講究録
第774巻 1991年 55-72

乱流間欠性の空間構造

京大 防災研 山田道夫 (Michio Yamada)
京大 数理研 大木谷耕司 (Koji Ohkitani)

1. Introduction

High Reynolds number fluid turbulence has long been a subject of extensive investigations. In 1941, Kolmogorov proposed a celebrated power-law of energy spectrum of turbulence. Since then, an enormous amount of studies have been performed to elucidate an underlying mechanism for the universal Kolmogorov spectrum. It is now widely accepted that the energy cascade process from lower to higher wavenumber is the most important dynamical process, through which a memory of the energy injection scale is lost and the universality of flow structure results at higher wavenumbers. However, this cascade process itself, sometimes called Richardson cascade, has been only a matter of theoretical consideration, and its hierarchical structure has not been clearly captured in experiments nor in numerical simulations.

Recently Argoul et al. applied to an experimental data of high Reynolds number turbulence a novel method of data analylsis, called wavelet analysis, which yeilds a time-frequency (space-wavenumber) diagram showing a pitchfork hierarchy of active regions (Argoul, Arneodo, Grasseau, Gange, Hopfinger and Frisch 198; Arnoedo, Grasseau and Holschneider 1989a,b; Arneodo, Argoul, Elezgaray and Grasseau 1989; Argoul, Arneodo, Elezgaray and Grasseau 1989; Everson et al. 1990; Farge and Rabreau 1988; Farge et al. 1989; Freysz et al. 1990; Ghez and Valenti 1989; Holschneider 1988; Chhabra et al. 1989; Vergassola and Frisch 1990). This diagram was taken to be the first experimental evidence of the Richardson cascade process. But later the application of the wavelet analysis to an artificial random noise was found to give a similar pitchfork hierarchy (Bacry, et al. 1989; Everson and Sirovich 1989; Ohtaguro 1990 (private communication)), which indicated that the pitchfork pattern in the wavelet analysis cannot be simply taken as an evidence of the Richardson cascade process and care should be taken of the interpretation the pitchfork pattern.

In this paper, we make use of the wavelet analysis to identify a trace of energy cascade process from an experimental data of atmospheric turbulence. In contrast to the case of Argoul et al., who used a continuous wavelet transform method with Mexican and French top hats, we here employ a discrete wavelet analysis (orthonormal wavelet expansion method) with an analyzing wavelet of Meyer type (Meyer 1989; Morimoto 1988) for a time-frequency analysis of the turbulence data. Our adoption of the orthonormal wavelet is based on the fact that the continous wavelets form an over-complete basis which necessarily brings about a formal relation between expansion coefficients (Grossmann and Morlet 1985; Grossmann Morlet and Paul 1985; Daubechies et

al. 1986; Liandrat and Moret-Bailly 1990), while the orthonormal wavelets form a complete orthonormal basis free from such kind of constraint on the expansion coefficients. Here we also apply the orthonormal wavelet analysis to an artificial random noise for comparison. First we comfirm several differences between turbulence data and random noise by making use of a relation between the orthonormal wavelet analysis and conventional scale analysis (Yamada and Ohkitani 1990). Then, we introduce a local wavelet spectrum constructed by the wavelet coefficients. For turbulence, it shows a similarity-pattern considered to correspond to the energy cascade process, while not for the random noise.

In Section 2 we describe the turbulence data to be analyzed in the following. In Section 3, conventional comparisons are made between the turbulence data and an artificial random noise by using the orthonormal wavelet expansion. Further comparisons are made by introducing the local wavelet spectrum in Section 4. We summarize the results in Section 5.

2. Fourier and wavelet spectra of turbulence

In this paper, we discuss an orthonormal wavelet analysis of a velocity signal in turbulence. The orthonormal wavelet expansion of a function f(t) takes the following form,

$$f(t)=\Sigma_j \Sigma_k \alpha_{j,k} \psi_{j,k} \qquad (1)$$

where $\alpha_{j,k}$ ($j,k\in Z$, where Z is the set of all integers) is an expansion coefficient and $\{\psi_{j,k} | j,k\in Z\}$ is a complete orthonormal set of wavelets generated from an analyzing wavelet $\psi(t)$ by descrete translations and discrete dilations. It is usual to take the discrete dilation in octaves, and to make the wavelets as

$$\psi_{j,k}(t)=2^{j/2}\psi(2^j t-k) \quad (j,k\in Z), \qquad (2a)$$

with the orthonormality condition

$$\int_{-\infty}^{\infty} \psi_{j,k}^{*}(t)\psi_{j',k'}(t)dt=\delta_{jj'}\cdot\delta_{kk'} \quad (j,k\in Z), \qquad (2b)$$

where δ_{ij} is the Kronecker's symbol. Note that j is the dilation parameter and k indicates the temporal position of time $k/2^j$. In order that $\{\psi_{j,k}\}$ may be a complete orthonormal basis (in $L^2(R)$), the analyzing wavelet $\psi(t)$ has to be carefully chosen. Some methods have been proposed so far to construct the analyzing wavelet (Battle 1987; Daubechies 1988; Lemarie 1988; Mallat 1988). Now we follow Meyer's procedure to obtain the analyzing wavelet. Here we do not go into its details, which should be found in Meyer(1985,1989), Morimoto(1988) and Yamada and Ohkitani(1990). We only mention that the wavelet spectrum E_j is related to the Fourier spectrum $E(\omega)$ of f(t) as

$$E_j \equiv \Sigma_k |\alpha_{j,k}|^2 \sim \omega E(\omega), (\omega\sim 2^{j+2}\pi/3). \qquad (3)$$

We remark that if the energy spectrum has a power law, so does the left hand side of (3), and vice versa,

$$E(\omega) \sim \omega^{-p} \quad <--> \quad E_j \sim 2^{-j(p-1)} \qquad (4)$$

At present, turbulent velocity data with highest Reynolds number can be obtained by geophysical or possibly astronomical observations, although they usually give only time series at a single or a few spatial points. The Reynolds number in these cases is at least one or two digits larger than those available in numerical simulation or in laboratoty experiment. Here we took a velocity singal of turbulence in the atmospheric boundary leyer, by a single hot-wire anemometer at a samplng frequency 500 Hz for over 3 minutes. The mean velocity was $U=\langle u(t)\rangle=5.4$ [m/sec] and the turbulence level was $u'/U=0.27$, where $u(t)$ denotes the velocity at time t, $\langle\rangle$ time average and $u'=\sqrt{\langle(u(t)-U)\rangle^2\rangle}$. The turbulence level is not very small, but we employ the Taylor's frozen hypothesis assuming that it is valid at least for small-scale of motion. Other turbulence parameters of interest are Kolomogorov's dissipation scale $\eta=[\nu^2U^2/15\langle(\partial u/\partial t)^2\rangle]^{1/4}=6.9\times10^{-4}$ [m], Taylor microscale $\lambda=u'U/\langle(\partial u/\partial t)^2\rangle^{1/2}=1.8\times10^{-1}$ [m], and the micro-scale Reynolds number $R_\lambda=u'\lambda/\nu=1.8\times10^4$, where $\nu=1.5\times10^{-5}$ [m^2sec^{-1}] is the kinematic viscosity of the air. We note that the validity of the Taylor hypothesis influences the accuracy of λ.

We show in Fig.1 the Fourier spectrum averaged over 80 samples, each of which was obtained from a time series of 10^{12} points. A power law consistent with an exponent -5/3 (Kolmogorov's spectrum) is observed over 2 decades of the wavenumber.# We note that for this high Reynolds number

---

Here no conditional sampling method is employed in contrast to the case of Yamada and Ohkitani(1990).

---

atmospheric turbulence, longer duration of the data sampling would yield a wider inertial subrange spectrum extending toward lower wavenumbers. At the highest wavenumber region the dissipation range is captured only marginally with this sampling frequency. However, this is not a significant drawback because here we are primarily interested in the velocity structure of the velocity field in the inertial subrange rather than at the dissipation wavenumbers.

The wavelet spectrum E_j with n=15 (with no averaging procedure) for the turbulence is shown in Fig.2 against j, where the logarithm of E_j to the base 2 was plotted for the direct assessment of the slope*. Remember that E^j is a sum of 2^j wavelet

---

*The index j now corresponds to $\omega\sim(500/2^{15})2^{j+2}\pi/3$.

---

coefficients, which implies that statistical fluctuations is significant for smaller j but not for larger j. The inertial subrange with the expected slope -2/3 was observed over 8 octaves (j=5~12) in accordance with that over 2 decades of -5/3 range in the Fourier spectrum. The dissipation range begins around j=13 where a fall-off of the wavelet spectrum is observed.

3.Turbulence and phase-randomized signal

In order to capture the energy cascade in fully-developed turbulence, here we have recourse to a comparison of the turbulence signal with its phase-randomized counterpart, which we obtained by the inverse transform of the Fourier coefficients of the original data after randomizing their phases uniformly over $[0,2\pi]$ with their amplitudes unchanged. In Fig.3 we show the signals of the turbulence and the phase-randomaized signal over a whole interval ($N=2^{15}$). We cannot distinguish them by merely looking at their appearances. The Fourier (or wavelet) spectra are identical between the turbulence and the phase-randomized signal, by the definition of the latter.

In fully-developed turbulence we have the energy cascade from lower to higher wavenumbers, which gives rise to a constant energy spectral flux throughout the inertial subrange on the average. In physical space, such a relation can be described in terms of the third-order structure functions as $\langle \delta u(r)^3 \rangle \sim r$, where $\delta u(r)=u(x+r)-u(x)$ is the longitudinal velocity difference. We can obtain a corresponding quantity T_j [‡‡] in terms of the orthonormal wavelet coefficients as

$$T_j = 2^{3j/2} \Sigma_k \alpha_{j,k}{}^3 . \qquad (5)$$

which should be proportional to 2^{-j} when $\langle \delta u(r)^3 \rangle \sim r$. Here we have made use of the fact that $\alpha_{j,k}\psi_{j,k}(t)$ expresses the velocity variation of scale j (at position $k/2^j$) and the amplitude of $\psi_{j,k}(t)$ is of order $2^{j/2}$. In Fig.4(a), Tj is shown in a log-

---

[‡‡] In a previous paper T_j was defined in terms of $|\alpha_{j,k}|$ rather than $\alpha_{j,k}$ (Yamada and Ohkitani 1990).

-linear plot for the case of turbulence. Only the positive values are shown. There are 5 points well on a straight line with slope -1. We note that the inertial subrange determined by the third-order structure function is narrower than that determined by spectrum, as pointed out in other experiments. In Fig.4(b) we plot (the positive values of) T_j for phase-randomized signal. As expected, its behavior is a mess with no power-law behavior. The behavior of T_j can therefore distinguish the turbulence from the phase-randomized signal.

Next, we are concerned with the probabilty density function (PDF) of velocity difference in physical space. The PDF of velocity in turbulence is known to be nearly Gaussian, whereas that of velocity derivative nearly exponential. Now the orthonormal wavelet coefficients $\alpha_{j,k}$ (multiplied by $2^{j/2}$) correspond to the velocity difference of spatial scale 2^{-j}. It is therefore of interest to examine how the PDF of wavelet coefficients changes from larger scale (lower j) to smaller scale (larger j). In Fig.5(a) we show the PDFs of the wavelet coefficients for $j=9\sim14$. Each PDF is normalized to have unit variance, and the solid curve shows the standard Gaussian ditribution with zero mean and unit variance. For smaller $j(\leq 11)$, the departure from Gaussian distribution is not so significant. But for larger j (≥ 12) the PDFs look nearer to exponential than to Gaussian. Remember that j=13 and 14 lie in the dissipation range. Similar results were obtained by the use of band-pass filtering of the numerical turbulence (She et al. 1988), and by studying PDF of velocity difference for various

spatio-temporal separations (Biskamp et al. 1990). On the other hand, the corresponding PDFs for phase-randomized signal naturallly has Gaussion distribution throught j=9∿14(Fig.5(b)), in accordance with the central-limit-theorem (Sanada 1990).

5. Local wavelet spectra

The Gaussian distribution of the wavelet coefficients for the phase-randomized signal and the non-Gaussian distribution for the turbulence reflect the difference in the spatial distributions of energy. In Fig.6, we show the spatial distribution of the squared wavelet coefficients (j=9∿12) for (a)turbulence and (b)the phase-randomized signal. We can see quite an intermittent distribution of energy in the case of turbulence, while the energy appears to be far less intermittent for the phase-randomized signal. These results support a view that the non-Gaussian statistics is associated with the intermittency. Also in Fig.6 we can observe that in the case of turbulence there is a strong correlations of the wavelet coefficients between octaves, while not for the phase-randomized signal. In order to reveal this difference more clearly, here we introduce the *local wavelet spectrum*. Recall that the (global) wavelet spectrum is defined as the sum of squared wavelet coefficients for each scale over all k, that is, over the whole interval (See Eq.(3)). To define local wavelet spectra, we first choose scale j_s. Then, the local wavelet spectrum $E_j{}^{k'}$ for scale $j(\geq j_s)$ at position k' is defined as a sum of squared wavelet coefficients over the subinterval corresponding to the spatial resolution at $j=j_s$. More specifically, we define

$$E_j{}^{k} = \Sigma' |\alpha_{j,k'}|^2 \quad \text{for } k=0\sim 2^{j_s}-1, \tag{6}$$

where Σ' denotes the summation over k' satisfying $k/2^{j_s} \leq k'/2^j < (k+1)/2^{j_s}$. Note that the sum of the local spectra over k recovers the (global) wavelet spectrum;

$$E_j = \Sigma_k E_j{}^{k}. \tag{7}$$

In Fig.7(a) we show the local wavelet spectra with $j_s=7$ for the turbulence in a perspective plot. We take as the height the logarithm (to the base 2) of $2^{j_s} \cdot E_j{}^{k'}$, where the factor 2^{j_s} normalizes the magnitude of the local wavelet spectrum to helpdirect comparison of the local wavelet spectra for different j_s. We can see characteristic strucures running in parallel with j-axis. Crests and troughs, that are observed at the lower wavenumbers in the inertial subrange (j=5∿12), penetrate deeply into the higher wavenumbers. We note that the plot looks highly irregular at j=14 in the dissipation range.

In Fig.7(b) we show the similar plot for the phase-randomized signal. The crests and troughs are observed at the smaller j(<7), but they disappear immediately toward larger j's, and the surface is quite uniform along k-axis at the scale of j=14. The prominent structure along j-axis in Fig.7(a) are, therefore, considered to originate from a substatial property of turbulence, rather than a formal property of the wavelet

expansion. Also in a numerical turbulence, the phase-randomization is found to suppress the vortex structures (She et al. 1990).

The phase-randomized signal does not include a structure corresponding to the energy cascade process in turbulence. Therefore, we consider that the prominent structures observed along j-axis in Fig.6(a) are traces of the energy cascade process in turbulence. It has been reported that continuous wavelet analysis gives similar branching patterns in the diagram of wavelet coefficients both for the turbulence and the artificial Gaussian signals**. In constrast, the present patterns in the perspective plots are clearly different between turbulence and

---

**Such comparison was suggested by Kraichnan (Bacry et al. 1989). Similar studies were done with the continuous wavelet analysis, independently by Everson and Sirovich (1989), and by Everson, Sirovich and Sreenivasan (1989) and by Ohtaguro (private communication 1990).

---

the phase-randomaized signal. At present, we cannot find a clear reason for the similar branching patterns observed by the continuous wavelet analysis. But the formal mutual dependence between continuous wavelet coefficients, originating from the non-orthogonality of the continuous wavelets, might lead to the branching pattern even in the case of phase-randomized signal. It might also make it difficult to decide whether the branching patterns is subtantial or formal in the case of turbulence. Continuous wavelet analysis using the present analyzing wavelet would be helpful to settle the matter.

As far as lower order quantities are concerned, the inertial subrange in turbulence has a statistical scale-similarity if a slight deviation due to intermittency is ignored (Anselmet et al. 1984). We can observe this similarity by comparing the overall view of the rescaled local energy spectra for different values of j_s (Fig.8), where the viscous effect reduces the magnitude of the spectrum at highest wavenumber range. These local wavelet spectra have similar structures, reflecting the scale-similarity of the inertial subrange. Because the phase-randomized signal has also no characteristic scale in the power-law range, it shows structures with scale-similarity, whose shapes are different from those of turbulence (Fig.9).

6. Summary

We applied the orthonormal wavelets to the data analysis of atmospheric turbulence which has a clear Kolmogorov spectrum. The orthonormal wavelet expansion has a merit that the basis functions are orthonormal and the mutual independency of the expansion coefficients are assured. Also the expansion coefficients are directly related to quantities examined in the conventional turbulence analysis.

In order to assure that substantial properties of turbulence are captured, we compared the results of the wavelet analysis for turbulence with those for an artificial phase-randomized signal. Both the third-order moments and the distribution function of the wavelet coefficients show a clear difference between turbulence

and the phase-randomized signal. Then we introduced the local wavelet spectrum to visualize the energy cascade process in turbulence. A characteristic structure over the inertial subrange is observed for turbulence, while not for the phase-randomized signal. This structure corresponds to be a trace of the energy cascade process in turbulence. Remark that the present orthonormal wavelets have distinguished the turbulence from the phase-randomized signal, while the continous wavelet does not appear to give a clear distinction between them.

The orthonormal wavelet coefficients also give quantitative information about scaling properties of moments of the vecolity field, which we will report in a separate paper.

Acknowledgements

We thank Professor U. Frisch for his helpful discussion and Professor L. Sirovich for sending his references. Thanks are also to Dr. Ohtaguro for his useful discussion.

References

Anselmet, F., Gagne, Y., Hopfinger E.J. and Antonia, R.A. (1984): J. Fluid Mech. **140**, 63.

Arneodo, A., Argoul, F., Elezgaray, J. and Grasseau, G. (1989): *Nonlinear Dynamics* (G. Turchetti ed.), World Scientific, p.130

Arneodo, A., Grasseau, G. and Holschneider, M. (1989a) : Phys. Rev. Lett., **61**, 2281.

Arneodo, A., Grasseau, G., and Holschneider, M. (1989b): *Wavelets* (Combes, J.M. et al. eds.), Springer, p.182.

Argoul, A., Arneodo, A., Elezgaray, J. and Grasseau, G. (1989): Phys. Lett., A**135**, 327.

Argoul, F., Arneodo, A., Grasseau, G., Gange, Y., Hopfinger, E. J. and Frisch, U. (1989): Nature, **338**, 51.

Bacry, E., Arneodo, A., Frisch, U., Gagne, Y. and Hopfinger E. J. (1989); *Turbulence and Coherent Structures*, Lesieur, M. and Metais, O. eds., Kluwer.

Battle, G. (1987): Commun. Math. Phys., **110**, 601.

Biskamp, D. , Welter, H. and Walter, M. (1990): Phys. Fluids B**2**, 3240.

Chhabra, A. B., Meneveau, C., Jensen, R. V. and Sreenivasan K. R. (1989): Phys. Rev. A**40**, 5284.

Combes, J.M., Grossmann, A. and Tchamitchian, Ph. eds. *Wavelets*, Springer, 1989.

Daubechies, I., Grossmann, A. and Meyer, Y. (1986) : J. Math. Phys. **27**, 1271.

Daubechies, I. (1988): Comm. Pure Appl. Math., **XLI**, 909.

Everson, R., Sirovich, L. and Sreenivasan, K.R. (1990): Phys. Lett. **145**, 314.

Everson, R. and Sirovich, L. (1989): Center for Fluid Mechanics, Brown University, Report, 89-182.

Farge, M. and Rabreau, G. (1988): C.R. Acad. Sci., II-**317**, 1479.

Farge, M., Holschneider, M. and Colonna, J.-F. (1989) : *Topological Fluid Mechanics* (Moffat, K. ed.), Cambridge Univ. Press, p.765.

Freysz, E., Pouligny, B., Argoul, F. and Arneodo, A. (1990): Phys. Rev. Lett., **64**, 745

Ghez, J.-M. and S. Vaienti (1989): J. Stat. Phys., **57**, 415.

Grossmann, A. and J. Morlet (1985): *Mathematics+Physics* (Streit, L. ed.), vol.1, World Scientific, p.135.

Grossmann, A., Morlet, J. and Paul, T. (1985): J. Math. Phys., **26**, 2473.

Grossmann, A., Kronland-Martinet, R., and Morlet, J. (1989): *Wavelets* (Combes, J.M. et al. eds.),Springer, p.2.

Holschmeider, M. (1988): J. Stat. Phys., **50**, 963.

Lemarie, P.-G. (1988): J. Math. Pure et Appl., **67**, 227.

Liandrat, J. and F. Moret-Bailly (1990): Eur. J. Mech., B/Fluids, **9**, 1.

Mallat, S.: Preprint GRASP Lab., Dept. of Computer and Information Science, Univ. of Pennsylvania.

Meyer, Y. (1985): Seminaire Bourbaki 1985/1986, n° 662.

Meyer, Y. (1989): *Wavelets* (J.M. Combes et al. eds.), Springer, p.21

Morimoto, A. (1988): Master thesis in Math. Dept. of Kyoto Univ.

Perrier, V. and C. Basdevant (1989): Rech. Aerosp., **3**, 53.

Sanada, T. (1990): Prog. Theor. Phys., **84**, 12.

She, Z.-S., Jackson, E., Orszag, S.A.(1988): J. Sci. Comp., **3**, 407.

She, Z.-S., Jackson, E., Orszag, S.A.(1990): Nature **344**, 226.

Vergassola, M. and U. Frisch (1990): preprint, submitted to Physica D.

Yamada, M. and Ohkitani, K. (1990): Prog. Theor. Phys., **83**, 819.

Figure Captions

Fig.1 The energy spectrum of the turbulence.

Fig.2 The wavelet spectrum of the turbulence.

Fig.3 The time series of (a) the turbulence u and (b) the phase-randomized signal u_r.

Fig.4 The third order structure function for (a) the turbulence (b) the phase-randomized signal.

Fig.5 The PDF's of the wavelet coefficients for (a) the turbulence and (b) the phase-randomized signal.

Fig.6 The spatial distribution of the wavelet coefficients for (a) the turbulence and (b) the phase-randomized signal.

Fig.7 The local wavelet spactra with $j_s=7$ for (a) the turbulence and (b) the phase-randomized signal. The whole interval of k'-axis corresponds to the whole data.

Fig.8 The local wavelet spectra for the turbulence with (a) $j_s=5$, (b) $j_s=7$. In (b) the spatial coordinate is expanded by a factor 4, in order to see the scale-similarity directly.

Fig.9 The local wavelet spectra for the phase-randomized signal plotted as in Fig.8.

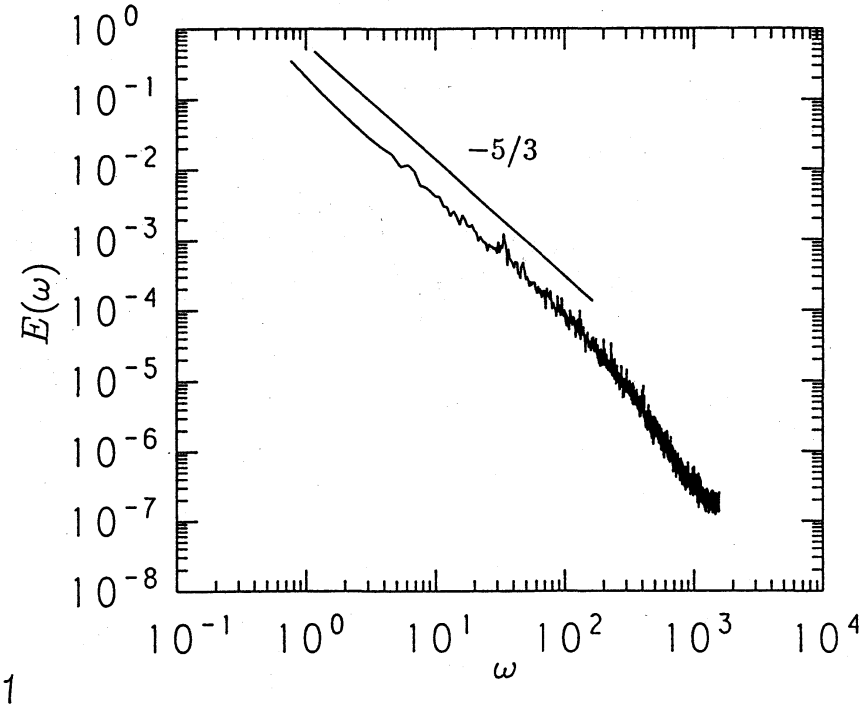
10^0
10^{-1}
10^{-2}
10^{-3}
10^{-4}
10^{-5}
10^{-6}
10^{-7}
10^{-8}
$E(\omega)$
−5/3
10^{-1} 10^0 10^1 10^2 10^3 10^4
ω

Fig. 1

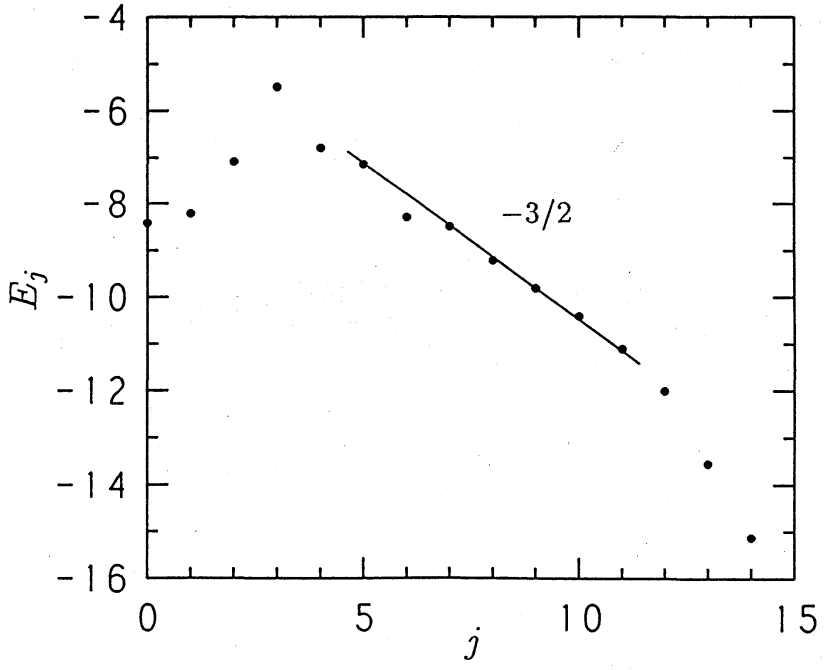
-4
-6
-8
-10
-12
-14
-16
E_j
−3/2
0 5 10 15
j

Fig. 2

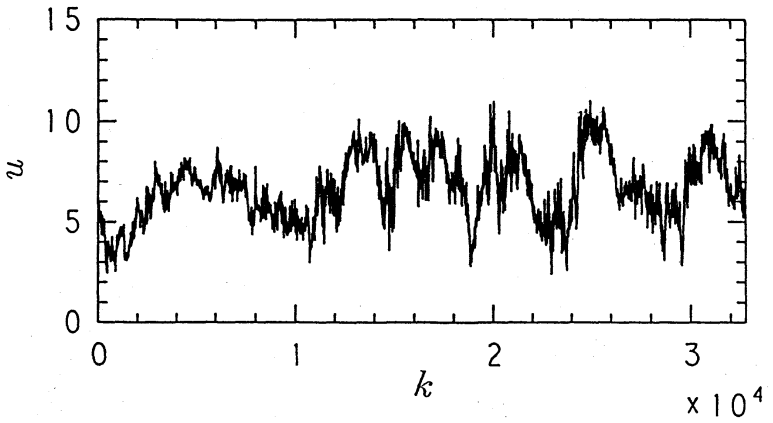

Fig.3(a)

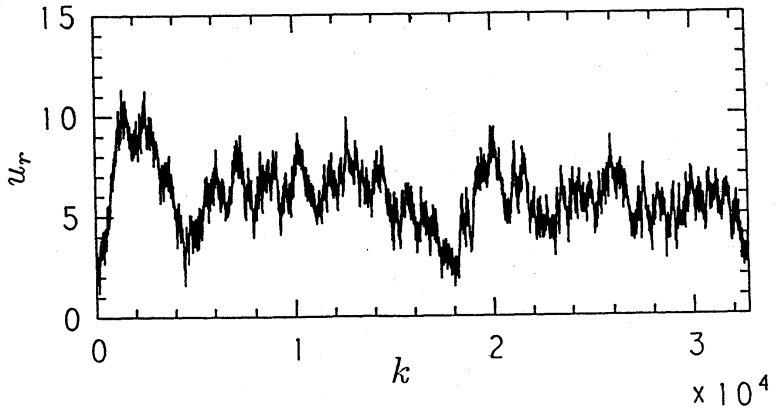

Fig.3(b)

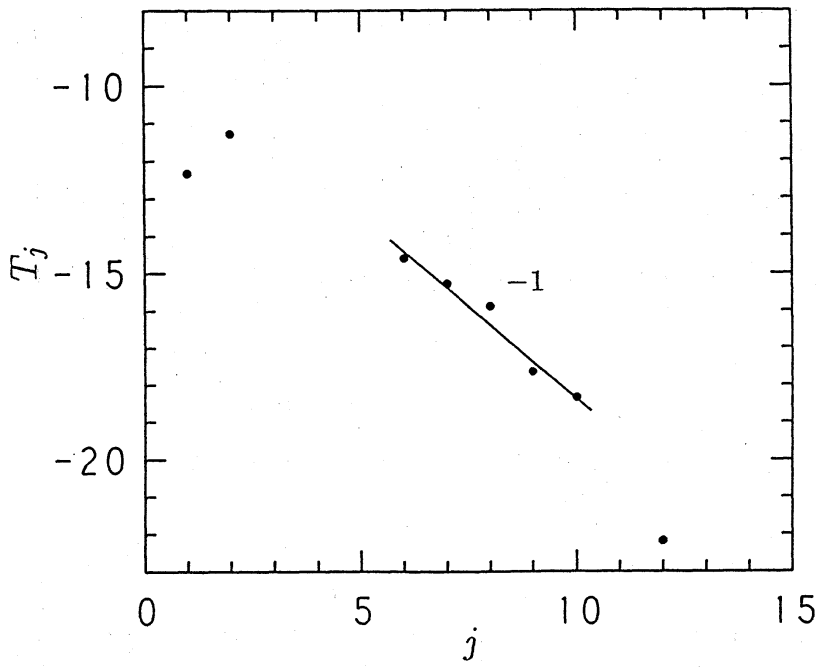

Fig.4(a)

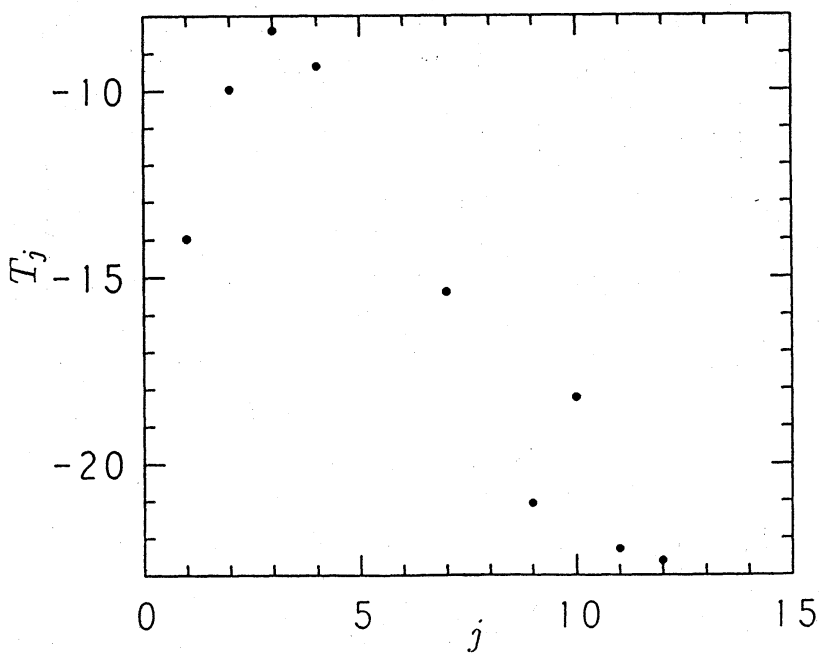

Fig.4(b)

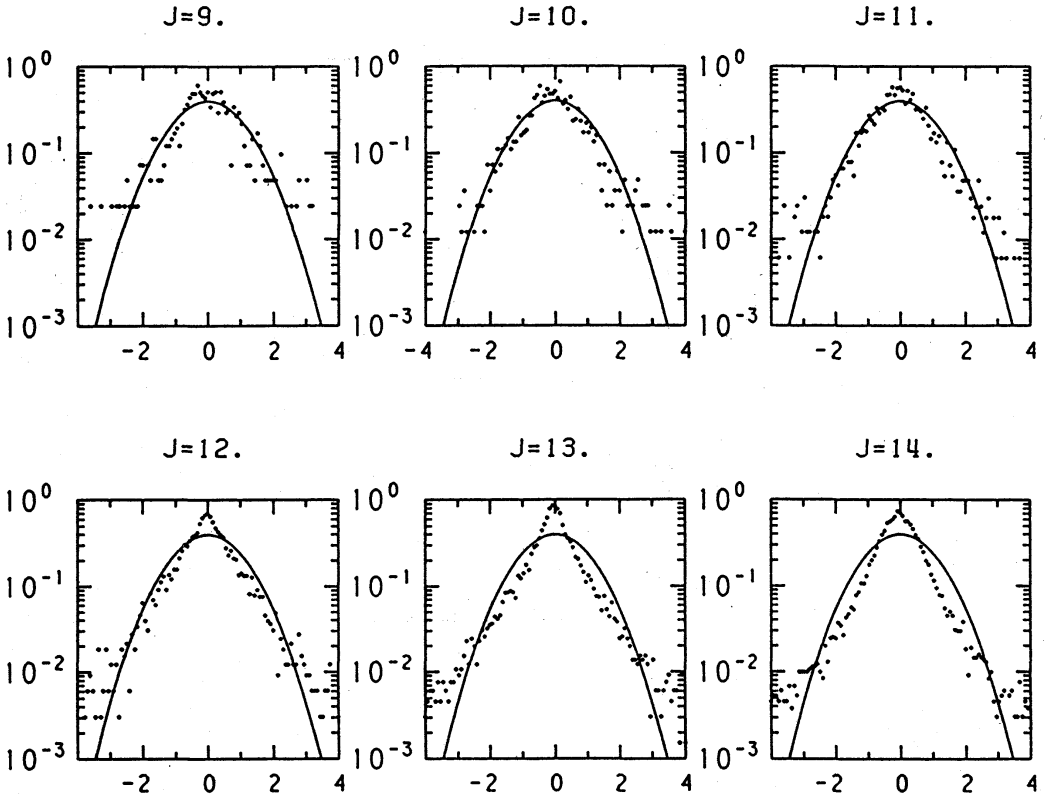
J=9.
J=10.
J=11.
J=12.
J=13.
J=14.
10^0
10^{-1}
10^{-2}
10^{-3}
-4
-2
0
2
4

Fig. 5(a)

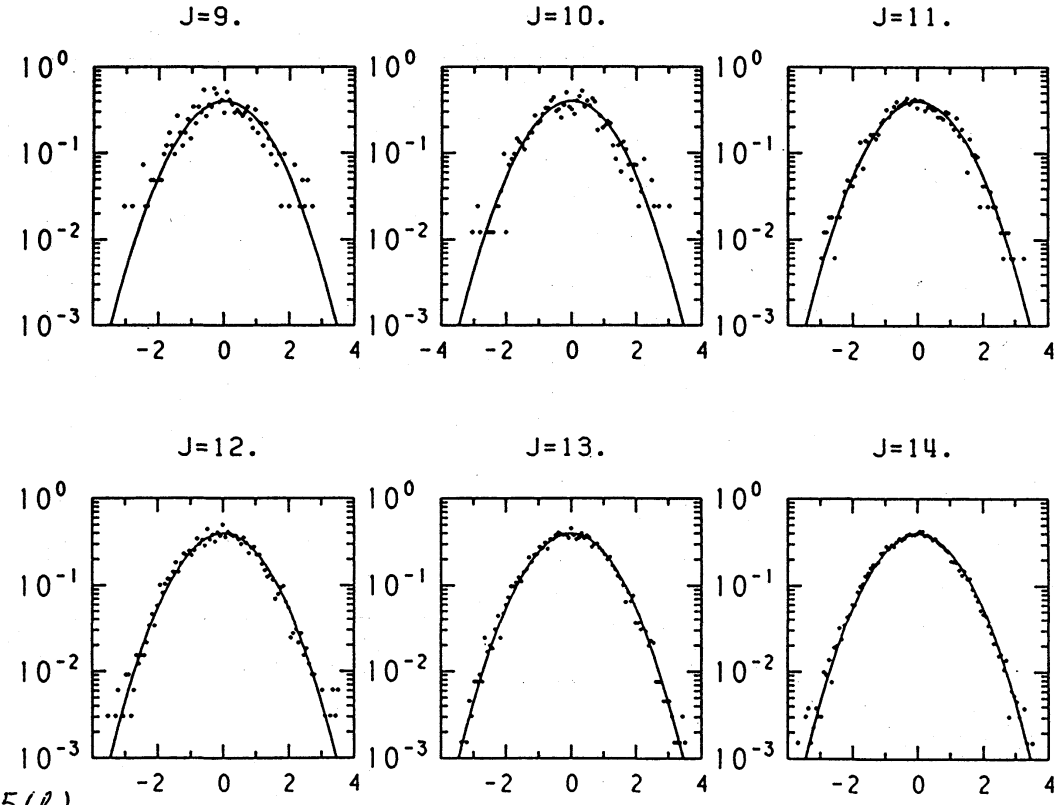
J=9.
J=10.
J=11.
J=12.
J=13.
J=14.
10^0
10^{-1}
10^{-2}
10^{-3}
-4
-2
0
2
4

Fig. 5(b)

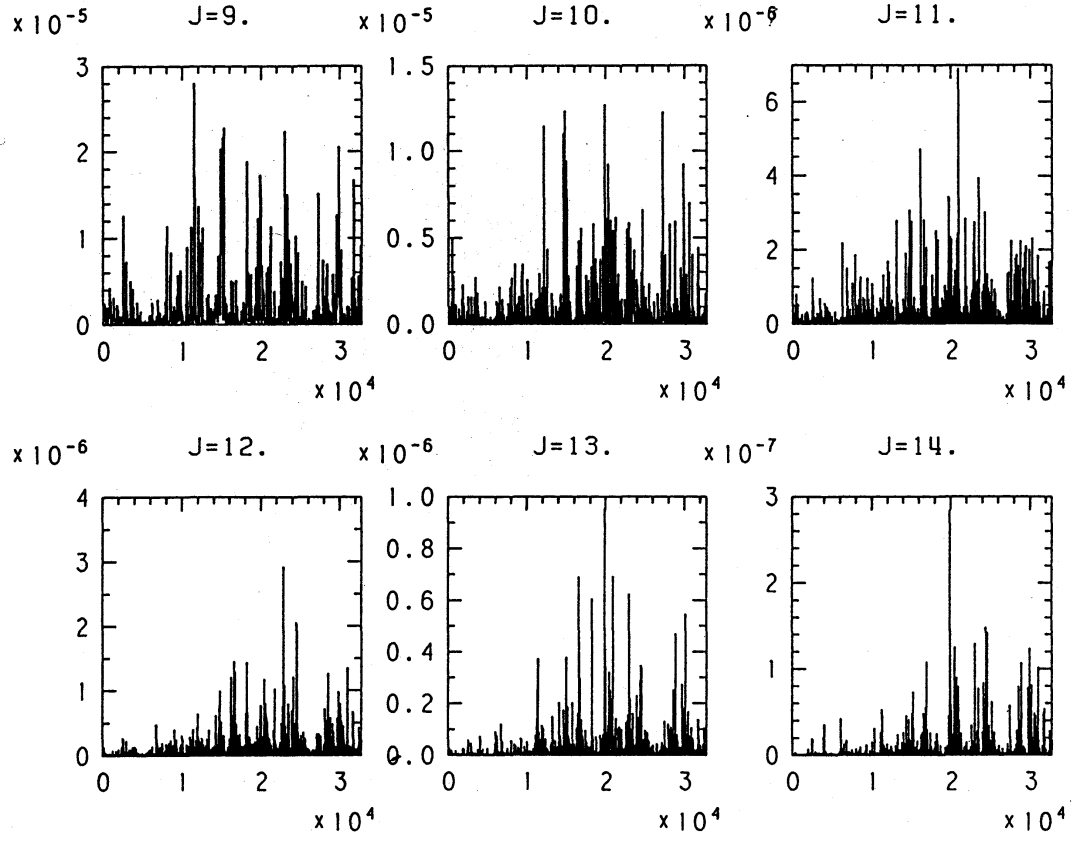
x 10^-5
J=9.
x 10^-5
J=10.
x 10^-6
J=11.
x 10^-6
J=12.
x 10^-6
J=13.
x 10^-7
J=14.
x 10^4

Fig.6(a)

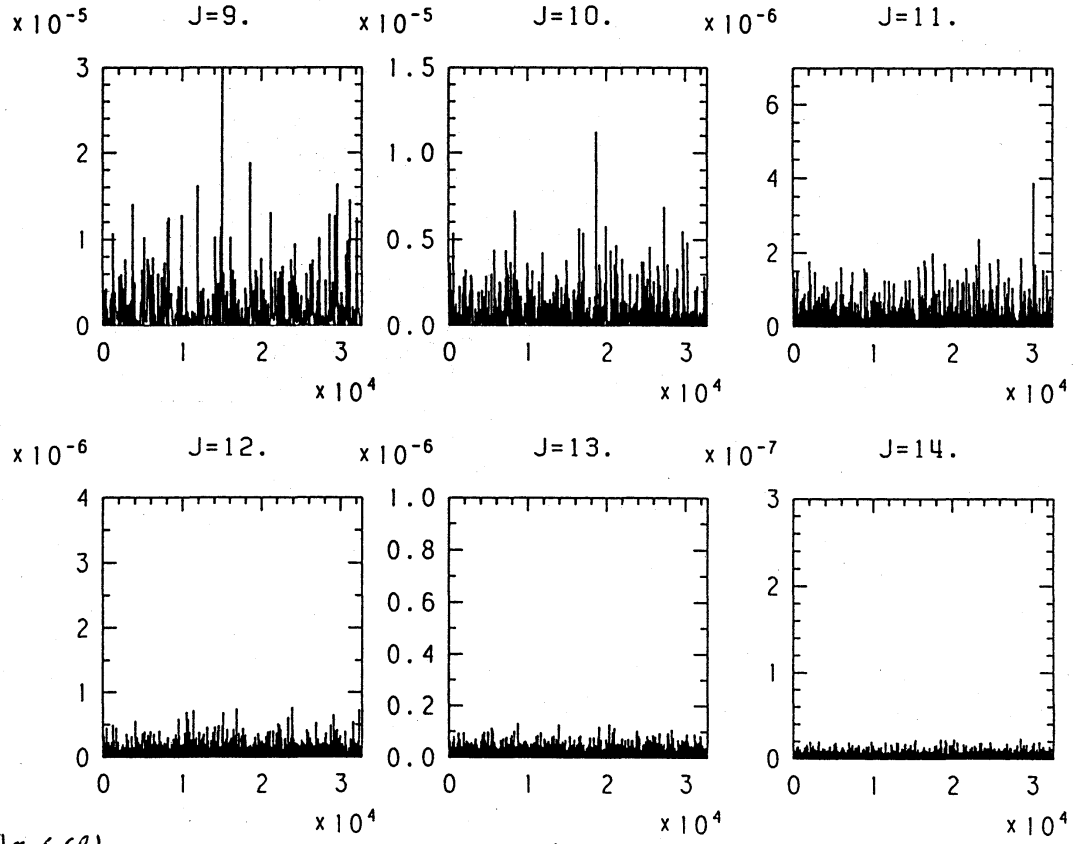
x 10^-5
J=9.
x 10^-5
J=10.
x 10^-6
J=11.
x 10^-6
J=12.
x 10^-6
J=13.
x 10^-7
J=14.
x 10^4

Fig.6(b)

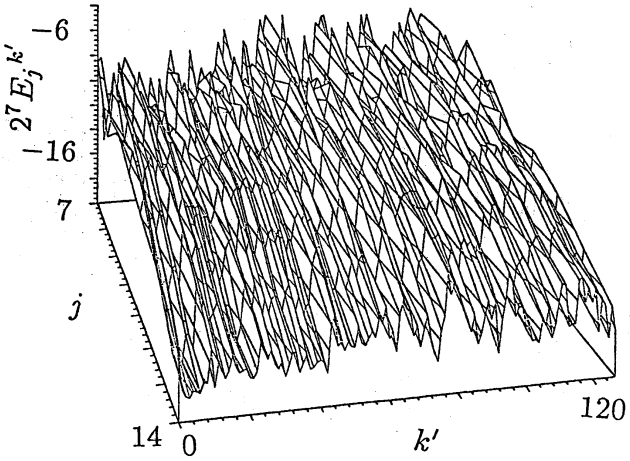

Fig. 7(a)

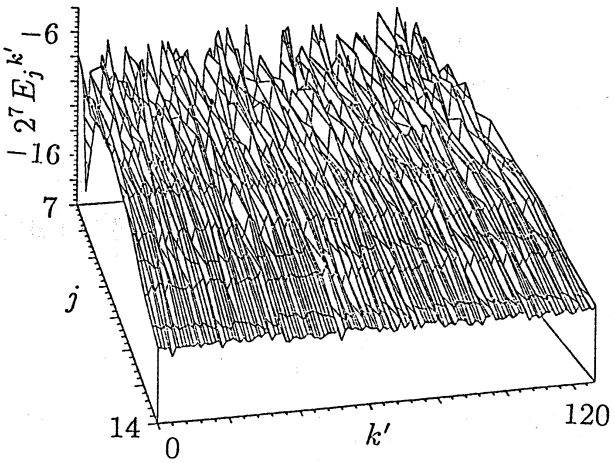

Fig. 7(b)

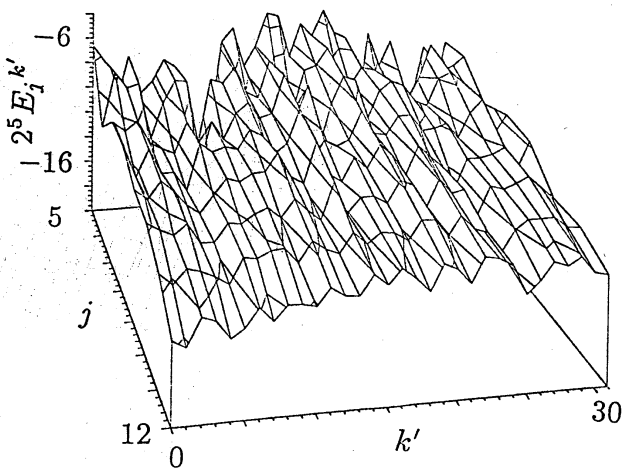

Fig.8(a)

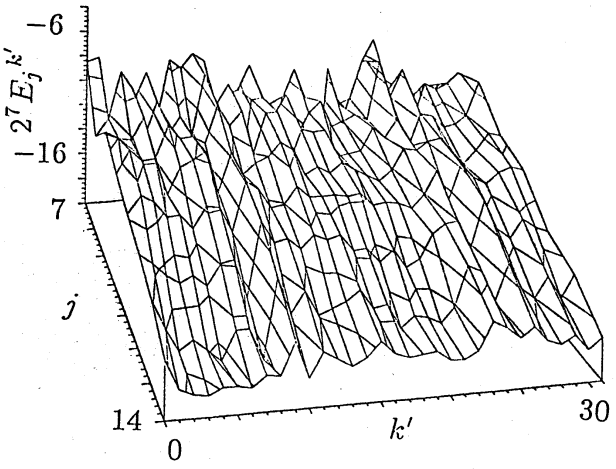

Fig.8(b)

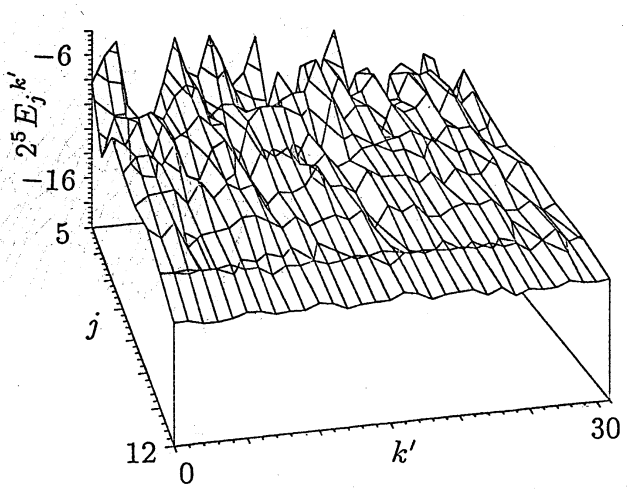

Fig. 9 (a)

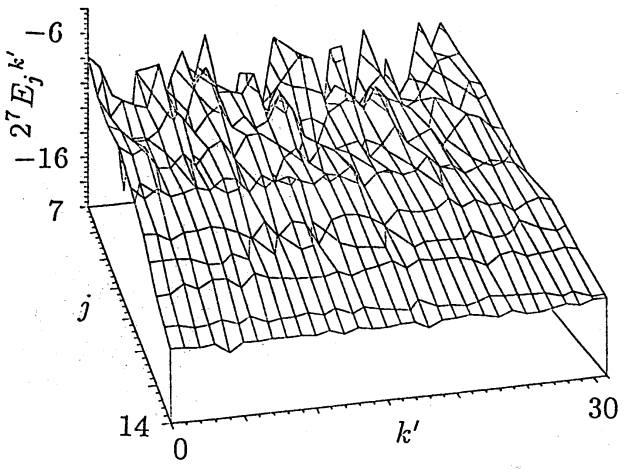

Fig. 9 (b)